ARTICLES
PUBLISHED ONLINE: 13 MAY 2012 | DOI: 10.1038/NPHYS2307
nature physics

Spin and valley quantum Hall ferromagnetism in graphene

A. F. Young[1]*†, C. R. Dean[2,3]†, L. Wang[3], H. Ren[1], P. Cadden-Zimansky[1], K. Watanabe[4], T. Taniguchi[4], J. Hone[3], K. L. Shepard[2] and P. Kim[1]*

Electronic systems with multiple degenerate degrees of freedom can support a rich variety of broken symmetry states. In a graphene Landau level (LL), strong Coulomb interactions and the fourfold spin–valley degeneracy lead to an approximate SU(4) isospin symmetry. At partial filling, exchange interactions can break this symmetry, manifesting as further Hall plateaus outside the normal integer sequence. Here we report the observation of a number of these quantum Hall isospin ferromagnetic (QHIFM) states, which we classify according to their real spin structure using tilted field magnetotransport. The large activation gaps confirm the Coulomb origin of all the broken symmetry states, but the order depends strongly on LL index. In the high-energy LLs the Zeeman effect is the dominant aligning field, leading to real spin ferromagnets hosting skyrmionic excitations at half filling, whereas in the 'relativistic' zero LL lattice scale interactions drive the system to a spin unpolarized state.

The low-energy effective theory of nearly neutral graphene describes two flavours of massless Dirac quasiparticles centred on the two inequivalent corners of the Brillouin zone, termed valleys. In a high magnetic field, the valley degeneracy combines with the physical electron spin to produce four component LLs, leading to the anomalous graphene quantum Hall sequence

$$\sigma_{xy} = \pm \frac{4e^2}{h}\left(N + \frac{1}{2}\right) \quad (1)$$

where e is the elementary charge, h is Planck's constant, the LL index N is a non-negative integer and the additional factor of one-half is related to the pseudospin winding number[1]. The spin–valley degeneracy makes graphene a prime candidate for observing the rich physics associated with multicomponent quantum Hall effects[2–4]. Graphene is exceptional as compared with its semiconductor counterparts owing to a near-perfect energetic hierarchy (Fig. 1b). The energy scales characterizing cyclotron motion (E_N) and long-range interparticle Coulomb interactions (E_C)—both of which reflect physics that is independent of spin or valley flavour—dwarf explicit spin and valley symmetry breaking effects. The combined four-flavour degeneracy can therefore be thought of as that of a single SU(4) isospin[5,6]. As in other multicomponent quantum Hall systems, exchange interactions can drive the system through a ferromagnetic instability[7], in which the order parameter corresponds to a finite polarization in a specific direction within the SU(4) isospin space. At integer fillings within a partially filled quartet LL, this order parameter is predicted to lead to a finite gap for charged excitations and a robust quantum Hall effect for integers outside the sequence described in equation (1). The precise SU(4) polarization for given experimental conditions depends on the interplay between anisotropies arising from the Zeeman effect, lattice scale interactions and disorder. All of these anisotropies are small and experimentally tunable, allowing for the possibility of a variety of distinct ground states across experimentally accessible ranges of filling factors, magnetic fields and realizations of disorder.

Previous studies have indeed reported observation of the QHE at several integer filling factors outside the normal sequence[8–13]; however, the nature of the (presumably broken symmetry) states leading to these plateaus remains a matter of intense theoretical debate[7,14–34]. In the $N = 0$ LL, most experimental[10,11,35–38] and theoretical[20–34] work has focused on the strongly insulating behaviour observed at $\nu = 0$, corresponding to half filling of the zero-energy LL, which has no analogue in conventional two-dimensional electron systems. The insulating state has been described variously as a spin polarized valley singlet, a valley polarized spin singlet or a lattice scale spin density wave, but experimental resolution of this discrepancy has been hampered by the absence of any probe of the spin or valley order. Even less is known about the symmetry breaking at $\nu = \pm 1$ (refs 8,9,15,17,18,23,39) or throughout the $N \neq 0$ LLs (refs 8,9,11,13). Owing to the anomalous structure of the N = 0 LL, in which the valley quantum number corresponds to a real-space sublattice, the symmetry broken states for $N = 0$ may not resemble those for $N \neq 0$; however, limitations on sample quality and geometry in SiO_2 supported and suspended devices, respectively, have precluded a comparative study.

In this article, we address these issues by studying the thermal activation gaps, $^{\nu}\Delta$, associated with the broken symmetry IQHE states in graphene devices fabricated on hexagonal boron nitride (hBN) substrates[12]. This gap is associated with energy cost of the lowest-lying charged excitations of the ground state. Owing to the atomic scale confinement of the electronic wavefunctions to the plane of the graphene, all orbital effects related to electronic interactions depend only on the out-of-plane component of magnetic field ($B_\perp$) whereas spins respond directly to the total magnetic field (B_T) independent of its direction. Tilted field measurements of the

[1]Department of Physics, Columbia University, New York, New York 10027, USA, [2]Department of Electrical Engineering, Columbia University, New York, New York 10027, USA, [3]Department of Mechanical Engineering, Columbia University, New York, New York 10027, USA, [4]Advanced Materials Laboratory, National Institute for Materials Science, 1-1 Namiki, Tsukuba, 305-0044, Japan. †These authors contributed equally to this work.
*e-mail: andrea@phys.columbia.edu; pk2015@columbia.edu.

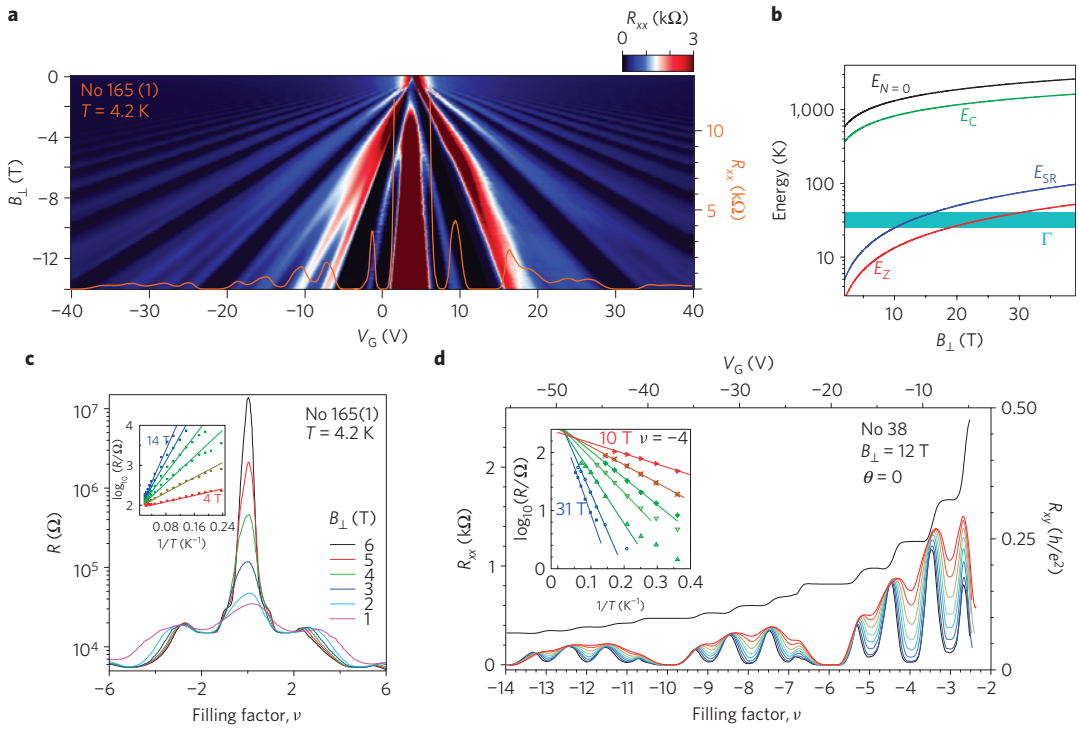

Figure 1 | All-integer quantum Hall effect in graphene on hBN. a, Landau fan from a monolayer graphene on hBN device. Symmetry breaking of the LLs is visible from a few tesla, and at $B_\perp = 14$ T (superimposed) all integer filling factors feature minima in R_{xx}. The colour scale for $-2 < \nu < 2$ has been expanded by a factor of seven. **b**, Energy scales. The cyclotron gaps ($E_N \simeq \hbar v_F \sqrt{2}/\ell_B$) and Coulomb energy ($E_C = e^2/\varepsilon\ell_B$) both characterize physics that does not distinguish between isospin flavours. The leading isospin anisotropies, which include the Zeeman effect ($E_Z = g\mu_B B_T$), lattice scale interactions ($E_{SR} \sim (a/\ell_B)E_C$; ref. 23) and disorder broadening (Γ), are at least one order of magnitude smaller. Here, $v_F \simeq 10^8$ cm s^{-1} is the Fermi velocity in graphene, $a = 2.46$ Å is the lattice constant, $g_0 = 2$ is the bare gyromagnetic ratio, μ_B is the Bohr magneton and $\ell_B \sim 26\,\text{nm}/\sqrt{B_\perp[\text{T}]}$ is the magnetic length. The disorder energy scale is extracted from the magnetic field dependence of the Shubnikov–de Haas oscillations at low magnetic field in one representative device (Supplementary Information). **c**, Development of the $\nu = 0$ insulating state. Inset: Temperature dependence showing the Arrhenius behaviour of the insulating resistance. **d**, Temperature dependence of the R_{xx} minima in the symmetry broken IQHE regime. Inset: Arrhenius plots for $\nu = 4$ as a function of magnetic field. The error bars are dominated by the uncertainty in the domain of the simply activated regime.

$^{\nu}\Delta$ thus enable us to extract quantitative information about the net spin of charged excitations in the broken symmetry states.

Figure 1a shows the evolution of the quantum Hall effect with magnetic field in a representative device (No 165 thermal cycle 1). Symmetry breaking at $\nu = \pm 1$ is visible at fields of $B_\perp \gtrsim 5$ T, followed by the higher LLs at $B_\perp \gtrsim 7$ T; by 14 T (overlaid), ρ_{xx} minima are visible at all integer fillings within the experimental range. In addition, an insulating state develops at $\nu = 0$ (Fig. 1c) starting from 2 to 3 T, consistent with previous work on clean, suspended graphene[11,37]. We find that all broken symmetry ρ_{xx} minima, as well as the $\nu = 0$ insulator, show simply activated temperature dependence over a wide range of fields (Fig. 1c and d, insets; note that Fig. 1d is data from a different device), enabling us to extract the energy gap $^{\nu}\Delta$ as a function of perpendicular and total field. The exceptional quality of the devices studied here enables the observation of all integer filling broken symmetry states at magnetic fields of a few tesla, enabling the Zeeman energy to be tuned across a wide range in experimentally realizable magnetic fields. Using this technique, we explicitly demonstrate the dependence of the isospin ferromagnetic order, for fixed relative filling, on LL index N. For $N \neq 0$ a dominant Zeeman anisotropy leads to spin polarized ground states at half filling and valley textured excitations at quarter filling, whereas in the $N = 0$ LL the situation is reversed: the $\nu = 0$ insulator is shown to be unpolarized, and real spin textures form the most favourable charged excitations from the fully polarized $\nu = 1$.

We start our discussion with the half-filled LLs. Figure 2a,d shows activation gaps for the half-filled LLs, $\nu = 0$, -4, -8 and -12, as a function of $B_\perp$. The perpendicular field dependence of $^{\nu}\Delta$ for all N is qualitatively similar, following an approximately linear scaling with $B_\perp$. We define the effective gyromagnetic ratio in perpendicular field from the slope of these curves, $g_\perp \equiv \mu_B^{-1}\partial_{B_\perp}(^{\nu}\Delta)$. We find that $g_\perp$ is enhanced with respect to the bare value $g_0 = 2$. The Coulomb energy is the only scale in the system compatible with the measured energy gaps, which are much larger than might be expected from known single-particle effects. Moreover, $g_\perp$ decreases with increasing LL index N, consistent with exchange-driven quantum Hall ferromagnetism[7].

Tilted field measurements reveal the uniqueness of the $N = 0$ LL. For $N \neq 0$, the half-filled gaps, $^{-4}\Delta$, $^{-8}\Delta$, and $^{-12}\Delta$, increase with B_T for fixed $B_\perp$ (Fig. 2d). This is consistent with the existence of real spin polarized states, in which excitations involve quasiparticles containing a net spin reversal relative to the ground state (and applied magnetic field). The activation gaps of such excitations consist of a direct Zeeman contribution from the reversal of spins against the external field, as well as an exchange contribution (Δ_X) arising from the spin reversal relative to adjacent (polarized) spins,

$$\Delta = \Delta_X(B_\perp) + g_0\mu_B B_T - \Gamma \qquad (2)$$

where Γ is the disorder broadening of the LLs and μ_B is the Bohr magneton. In contrast, the $\nu = 0$ resistance decreases (Fig. 2b with increased B_T, an observation incompatible with the real spin polarized scenario for $\nu = 0$ (refs 22,25,28,31). Instead, the data suggest that a spin unpolarized state, in which excitations contain a net spin aligned parallel (rather than antiparallel) to the applied field, underlies the insulating behaviour at $\nu = 0$.

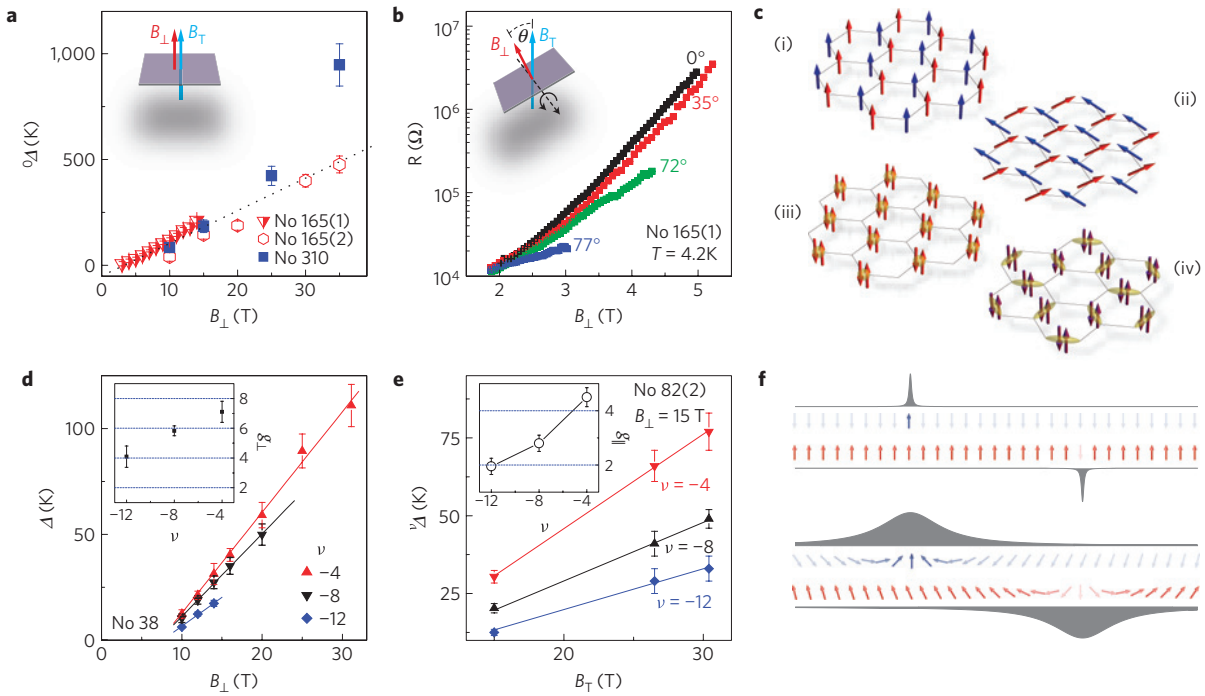

Figure 2 | Activation gaps of half-filled quartet LLs. a, $B_\perp$ dependence of the $\nu = 0$ gap, ${}^0\Delta$, for several devices. ${}^0\Delta$ increases approximately linearly with applied $B_\perp$, a feature not associated with any currently proposed theory for $\nu = 0$. The dashed line indicates $g_\perp = 23$. **b**, Tilted field dependence of the resistance of the $\nu = 0$ state. The resistance increases exponentially with field, consistent with a gapped state with ${}^0\Delta \propto B_\perp$. The resistance at fixed $B_\perp$ decreases for higher tilt angles, indicating a spin-unpolarized state. **c**, Candidate QHIFM states for $\nu = 0$. Our experiment rules out the spin ferromagnet, (i); all other states are marked by lattice scale spin (for the canted antiferromagnet (ii)) or charge (for the charge density wave (iii) or Kekulé distortion (iv)) order. **d**, $B_\perp$ dependence of the half-filled quartets for $N \neq 0$, $\nu = -4, -8, -12$. Like the $\nu = 0$, all gaps scale approximately linearly with $B_\perp$, with enhanced $g_\perp$ factors that decrease with increasing LL index. **e**, Unlike the $\nu = 0$ state, all activation gaps measured for half-filled LLs with $N \neq 0$ increase with B_T, indicating spin polarized states. For $\nu = -4$ and -8, the enhancement of $g_\parallel$ indicates that charged excitations contain multiple flipped spins. **f**, Schematic representation of charged excitations at half filling for $N \neq 0$. Excitations into the spin-reversed conduction band can take the form of single reversed spin particle–hole pairs or smoothly varying skyrmion–antiskyrmion (S–aS) spin textures, depending on the strength of exchange interactions relative to disorder and the Zeeman energy. At $B_\perp = 15$ T in the samples studied in this work, the S–aS scenario prevails at $\nu = -4$ and -8, whereas charge at $\nu = -12$ is carried by single electron–hole pairs. The error bars on all activation gaps are dominated by the uncertainty in the range of the simply activated regime, which is much larger than intrinsic scatter in the data.

Half filling of a fourfold-degenerate graphene LL provides an ideal testing ground for the relative strength of the spin and valley anisotropies within the SU(4) isospin space. Because each cyclotron guiding centre is doubly occupied, Pauli exclusion prevents the half-filled LL from fully polarizing in both spin and valley simultaneously. As a result, spin and valley polarizing tendencies necessarily compete, and the resulting ground state reflects the result of this competition. The fact that different orders prevail at half filling for $N = 0$ and $N \neq 0$ even under identical experimental conditions ($B_\perp$ and B_T, which together fix the relative magnitude of the real spin anisotropy) suggests that the difference between LLs is intrinsic to graphene and originates in the valley sector. A likely origin lies with the unique structure of the ZLL wavefunctions: whereas for the $N \neq 0$ LLs wavefunctions in a single valley are spread equally over the two real space sublattices, for the ZLL electrons in a single valley are localized on a single sublattice[6]. Long-range interactions do not distinguish between such lattice scale orbital structural difference, but short-range interactions do, potentially leading to different ground states in the $N = 0$ and $N \neq 0$ LLs (ref. 23). At $\nu = 0$, the resulting interaction induced valley anisotropies have been predicted to drive the system to one of a number of sublattice-ordered ground states[20,21,23,24,27,29,30,33,34], some of which are depicted in Fig. 2c. The experimental data presented here indicate that, whereas the Zeeman effect wins the competition for the $N \neq 0$ LLs, leading to spin polarized states at $\nu = -12, -8$, and -4, the valley anisotropies dominate the zero LL, leading to the formation of one of the possible lattice scale density waves portrayed in Fig. 2c(ii)–(iv). The large size of the measured ${}^0\Delta$ gap, and its insensitivity to in-plane fields, suggest that the valley anisotropies may be more than ten times stronger than their naive scale, $(1/\ell_B) \times E_C$, in line with renormalization group[34,40] and numerical calculations[29].

A further notable feature of the experimental data is the linear dependence of ${}^0\Delta$ on $B_\perp$. The $\nu = 0$ insulating state is not spin polarized, precluding linear-in-B_T Zeeman contributions to the excitation energy (as in equation (2)); consequently, the linear dependence must have an orbital origin. Theoretical models based on Coulomb interactions within the continuum Dirac model, whereas consistent with the magnitude of the gaps, implicitly predict a $\sqrt{B_\perp}$ scaling of the $\nu = 0$ energy gap, a fact that derives from the $\sqrt{B_\perp}$ dependence of both E_C and E_0. Theories based on other mechanisms that do predict a linear dependence[18,26] are unable to account for the large ${}^0\Delta$ gap sizes observed.

Motivating future work on the $\nu = 0$ state, quantitative data (Supplementary Information) on the decrease of the gap in applied parallel field suggest that the real spin ferromagnet, which is predicted[22,25] to be an analog of the quantum spin Hall state[41], may be experimentally accessible in the best samples at high tilt angles in realistic magnetic fields ($B_T \lesssim 45$ T).

Despite the role of the single-particle Zeeman effect in setting the order in the higher LLs, tilted field activation gaps demonstrate

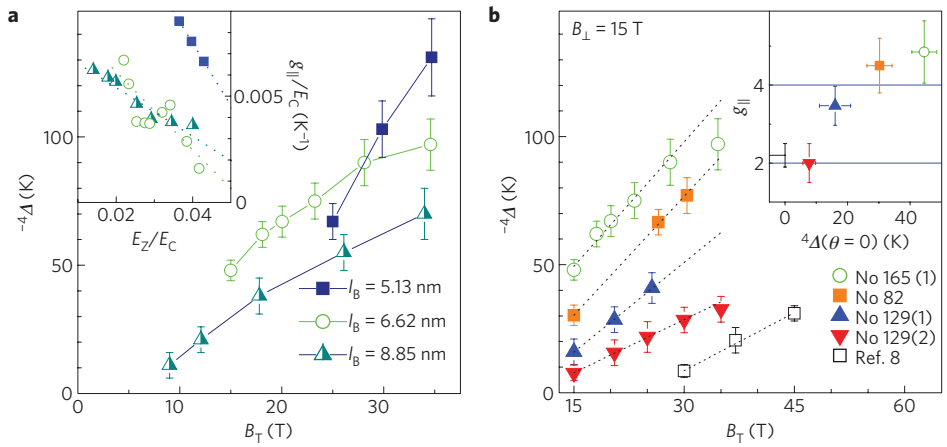

Figure 3 | Skyrmion transport at $\nu = -4$. a, Perpendicular field dependence of $g_\parallel$ at $\nu = -4$. The three curves show tilted field dependence of $^{-4}\Delta$ for three different values of ℓ_B. $g_\parallel$, calculated from nearest-neighbour and next-to-nearest-neighbour finite differences of the curves in the main panel, is negatively correlated with E_Z/E_C for fixed ℓ_B. For fixed E_Z/E_C, $g_\parallel$ is negatively correlated with ℓ_B, probably a combined effect of the increased exchange energy and decreased disorder parameter, Γ/E_C. Lines are guides for the eye. **b**, Device dependence of $^{-4}\Delta$ for $B_\perp = 15$ T. Cleaner devices show both larger activation gaps (at all fillings) and larger $g_\parallel$ for fixed ℓ_B. This trend is observed both across devices and for the same device on different cooldowns, for example device 129. The inset shows the device dependence of $g_\parallel$, which decreases with increasing disorder (for which $^{-4}\Delta(\theta = 0)$ serves as a proxy variable). Error bars arise from uncertainty in the range of the simply activated regime.

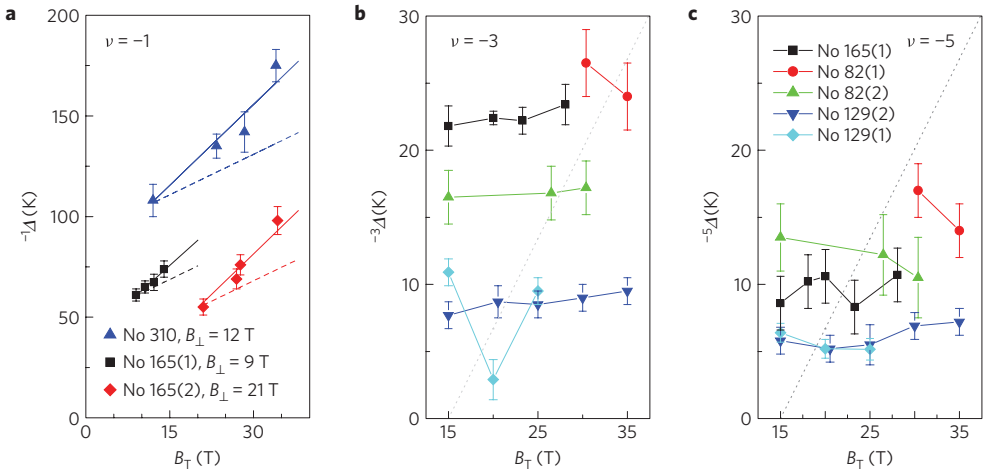

Figure 4 | Transport phenomena at quarter filling. a, $\nu = -1$. Energy gaps increase with B_T, suggesting that excitations from the expected spin polarized, sublattice polarized state[15,17,23] involve real spin flips. The dependence on B_T seems to support enhancement of $g_\parallel$ (solid lines are best linear fits to the data; dashed lines show $g_\parallel = 2$ for reference). **b**,**c**, Tilt dependence of $\nu = -3$ and $\nu = -5$. Most samples show minimal dependence on B_T, consistent with theoretical predictions of valley textured excitations[14]. It is likely that, in the absence of a single particle coupling field, these valley skyrmions may be large[50,51]. Note reentrant behaviour in sample No 129 (Fig. 5). Dashed lines show $g_\parallel = 2$ for comparison.

that the symmetry breaking can be thought of as being essentially spontaneous, with the Zeeman contribution functioning as a small aligning field. The gaps at half filling for $N \neq 0$ increase with total magnetic field (Fig. 2e) faster than might be expected for single spin flips, as reflected by the enhanced measured values of $g_\parallel \equiv \mu_B^{-1}\partial_{B_T}\Delta$ (Fig. 2e, inset). In a Zeeman dominated spin polarized state, charge transport occurs through the thermal activation of spin reversed particle–hole pairs (equation (1)). Whereas exchange contributions to the energy gap (the first term in equation (1)) lead to $g_\perp > g_0$ (ref. 42), this enhancement does not carry through to $g_\parallel$: changing B_T with $B_\perp$ fixed results in a measurement of the net spin of the excitation, and thus $g_\parallel = g_0$. In contrast, in exchange dominated spin polarized states it can be more energetically favourable to flip multiple spins smoothly in a skyrmionic spin texture[43,44], leading to a modified gap equation

$$\Delta = \Delta_X(B_\perp, K) + (2K+1)g_0\mu_B B_T - \Gamma$$

where $K \geq 0$, the extra flipped spins per charged excitation, depends on the ratio E_Z/E_C. The observed $g_\parallel > 2$ enhancements imply that $K > 0$ skyrmions constitute the charge carrying excitations at $\nu = -4$ and $\nu = -8$.

The widely tunable field effect natural to graphene facilitates the study of transport phenomena over a wide range of density in the same sample, enabling a detailed analysis of the dependence of $g_\parallel$ on LL index and $B_\perp$. Our data are qualitatively in line with theoretical expectations for skyrmion transport. The decreasing trend in $g_\parallel$ with increasing LL index reflects the trend in exchange energy[14]. In contrast to two-dimensional electronic systems with parabolic dispersion, where skyrmions are expected only in the lowest-energy LL (refs 43–45), skyrmions are theoretically possible for all $|N| \leq 3$ in monolayer graphene[14] for vanishing E_Z. We observe signatures of skyrmions up to $N = 2$, consistent with the presence of a finite Zeeman effect. Measurements of $g_\parallel$ at fixed filling for different values of $B_\perp$ in a single sample (Fig. 3a) show the expected decrease

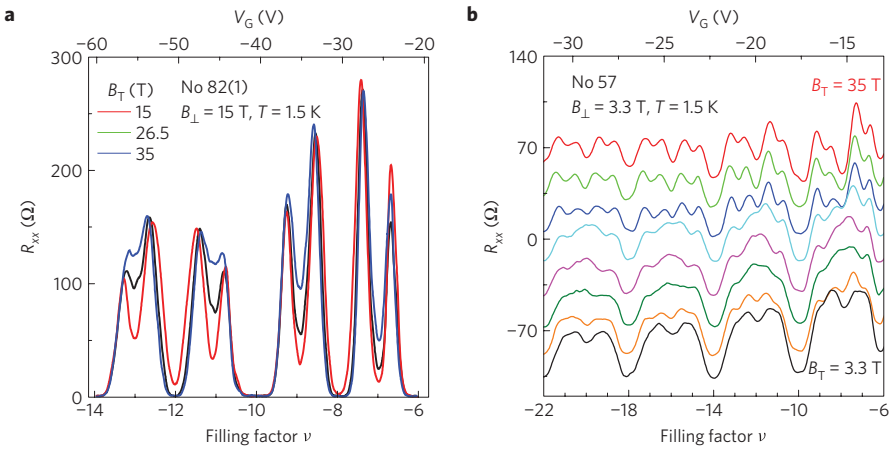

Figure 5 | Reentrant QHE in tilted field in the higher LLs. a, Gap collapse at odd filling. Gaps at quarter filling in the $N \neq 0$ LLs collapse in applied in-plane field in selected samples. Gap collapse, or collapse and reemergence (see $(-3)\Delta$ in device 129(1), Fig. 4) is device dependent. In the two devices in which it was observed, the behaviour did not survive a subsequent cooldown. **b**, At very low perpendicular magnetic fields, a further minimum is visible only at half filling. With the addition of an in-plane field, this minimum disappears, before reemerging again as B_T is increased further. Simultaneously, minima at quarter filling emerge with increasing B_T, indicating that they too can be spin active, increasing with B_T.

in $g_\parallel$—for fixed E_C—with increasing E_Z: the Zeeman coupling punishes large skyrmions, driving down K and, consequently, $g_\parallel$. However, our data do not conform to the clean skyrmion model, which predicts a universal scaling of the skyrmion energy with the dimensionless parameter E_Z/E_C. The inset of Fig. 3a shows the normalized in-plane dielectric constant, $g_\parallel/E_C$, for three different values of $B_\perp$ as a function of E_Z/E_C. Whereas the two lower $B_\perp$ curves collapse onto one another, in accordance with theoretical expectations for the clean limit, the $B_\perp = 25$ T data deviate strongly, implying the skyrmions are larger than predicted[3,43,44]. The failure of a universal scaling with E_Z/E_C suggests that a second dimensionless parameter, perhaps related to the disorder strength (for example, Γ/E_C), may be relevant for skyrmion transport[46].

We investigate the role of disorder in more detail by comparing several samples of varying quality. Overall, the values of $g_\parallel$ observed in our graphene samples are lower than those measured—for similar values of E_Z/E_C—in lower-disorder GaAs quantum wells[45]. Moreover, we find that $g_\parallel$ is sample quality dependent. Figure 3a shows the tilted field dependence of $^{-4}\Delta$ at $B_\perp = 15$ T for several devices with different amounts of disorder. Although higher disorder is correlated with smaller LL gaps, consistent with an increased LL broadening Γ, disorder also leads to a smaller measured $g_\parallel$. In the most disordered samples measured here, we find that $g_\parallel \approx 2$, matching a previous measurement of SiO_2 supported graphene[8] and implying that in disordered samples current is carried by single spin reversed particle–hole pairs. We speculate that skyrmion size may be principally limited not only by the Zeeman effect but also by the disorder landscape, which may tend to favour smaller skyrmion size[46]. The interplay between disorder and exchange may also contribute to the scaling of $g_\parallel$ with $B_\perp$ (Fig. 3a), which served to reduce the skyrmion radius, $r_{sky} \propto (2K+1)\ell_B$ (ref. 3), in comparison to the length scale characterizing the disorder potential landscape.

Like half filling, the phenomenology of a quarter-filled graphene LL also shows markedly different behaviour for $N = 0$ and $N \neq 0$. At quarter filling the naive ground state is a fully polarized state in which a single spin–valley flavour is occupied. Whereas spin is always polarized in the direction of the field, valley anisotropies are thought to lead to Ising or x–y type valley polarizations for $N = 0$ and $N \neq 0$, respectively[15,17]. Unlike the case at half filling, spin and valley anisotropies do not compete with each other in the formation of the ground state at quarter filling: for a singly occupied cyclotron guiding centre, there is no Pauli exclusion restriction on simultaneous spin and valley polarization. The interplay between spin and valley anisotropies does, however, contribute to the energetics of the excitation spectrum relevant for charge transport. In the case of a dominant Zeeman effect, for example, the low-lying charged excitations are thought to consist of valley flip textures[14] owing to the high relative energetic cost of flipping real spins against the physical field. Most (although not all) activation measurements taken at quarter filling for $N \neq 0$ (Fig. 4b,c) are consistent with this scenario, with the gaps independent of B_T for fixed $B_\perp$ to within experimental error. In contrast, gaps at $\nu = -1$ increase with increasing E_Z (Fig. 4a), suggesting again that the Zeeman effect is not the dominant anisotropy in the zero-energy LL. The tilted field dependence of the gaps at $\nu = -1$ also shows enhancement of $g_\parallel$ over the bare value, consistent with the large strength of exchange in the zero LL (ref. 14).

Whereas most data taken at half and quarter filling fit into the picture of QHIFM with LL index dependent anisotropy, we have observed several unexpected tilted field anomalies at both odd and even filling in the high LLs. For example, among samples for which $^{-3}\Delta$ was measured as a function of E_Z, one (129(1)) shows reentrant behaviour, with the gap collapsing with increasing Zeeman contribution and then growing again as E_Z is further increased. Qualitatively similar behaviour involving gap collapse in parallel field was observed in other samples throughout the quarter-filled $N \neq 0$ LLs (Fig. 5b). Reentrant behaviour was also observed at half filling in the higher LLs at low values of $B_\perp$ in one particularly high-mobility sample (Fig. 5b). The origin of this unexpected behaviour is not known, and the phenomenology is sample dependent. Although unlikely to be an intrinsic property of clean graphene, the reentrance tends to appear in cleaner samples, and disappears on sample contamination. One possible explanation is disorder[15,30,39], which can stabilize spatially inhomogeneous ground states whose manifestations may depend on the disorder realization in our small samples. Alternatively, the hBN substrate is known to give rise to long-wavelength potential modulations in the graphene[47], which may affect the broken symmetry states. This effect depends strongly on the relative orientation of the hBN and graphene lattices, which is random in the samples studied here, possibly accounting for the sample dependence of the reentrant behaviour.

The picture that emerges from our observation of spontaneously broken symmetry in monolayer graphene is one of exchange-driven quantum Hall ferromagnetism within the combined spin–valley isospin space[7], where the leading anisotropies differ between the

$N = 0$ and $N \neq 0$ LLs. Several questions remain, however: first, the precise nature of the $\nu = 0$ state remains elusive, and the linear $B_\perp$ dependence is unaccounted for theoretically. Moreover, the absence of spin polarization at $\nu = 0$ and the presence of spin-reversed excitations at $\nu = 1$ need to be reconciled with the prevailing theoretical models of the fractional quantum Hall effect graphene $N = 0$ LL (refs 48,49), all of which ignore the role of the valley anisotropies. Finally, little is understood about the structure and excitation spectrum of the odd filling states, and in particular the anomalous tilted field dependence observed in certain samples. We expect that the preliminary results presented here should motivate future work combining transport and surface science techniques, such as controlled absorption and scanned probe microscopy, to both elucidate the properties of these correlated states and, more generally, to use the graphene QHIFM as a model material platform for the systematic study of interacting systems in which all relevant experimental parameters, including disorder, can be tuned and probed *in situ*.

Methods

We follow the fabrication method described in refs 12,13 to produce multiterminal Hall bar and van der Pauw graphene devices on hBN substrates. Most devices presented were etched into the Hall bar geometry using a short exposure to O_2 plasma; all samples were annealed in a 5% H_2/95% Ar atmosphere to at 350 °C for several hours to remove processing residues. Typical sample sizes ranged from 0.5×0.5 to $5 \times 5\,\mu$m.

Devices were measured in a sample-in-^{4}He vapour variable temperature cryostat fitted with a mechanical sample rotation stage, mounted in the bore of a 35 T resistive magnet at the National High Magnetic Field Laboratory (NHMFL) in Tallahassee, Florida. Electrical measurements for $\nu \neq 0$ were made in the four-point geometry using a 10–100 nA current bias. For $\nu = 0$ measurements were taken in the two-terminal geometry using a 200 μV excitation voltage. The numerous features present in a gate voltage trace at intermediate magnetic fields ($B_\perp < 25$ T) enabled precise angle calibration, with $B_\perp$ determined to better than 0.5% accuracy. This was particularly important in the case of the $\nu = 0$ state, where the dependence on $B_\perp$ is at least one order of magnitude stronger than that on B_T.

R_{xx} minima were determined by sweeping the gate voltage at fixed temperature. All ρ_{xx} minima, as well as the resistance maximum at $\nu = 0$, obey an Arrhenius law, $R_{xx} \sim R_0 \exp(-\Delta/2T)$. Gaps were determined by fitting to this formula over at least one decade of resistance when possible. Error bars are dominated by ambiguity in picking out the appropriate 'linear regime'. Plots for all gaps presented in the main text, including best fits, are available in Supplementary Information.

Under normal conditions, samples of graphene on hBN are stable, and activation gaps can be measured repeatedly in the same sample over multiple cooldowns separated by weeks or months. However, rapidly warming the sample chamber causes outgassing from the cryostat walls, leading to the adsorption of debris on the graphene surface and higher disorder. This process, although difficult to control and not reliably reversible, enables us to exclude device-specific effects stemming, for example, from the interplay between the graphene electrons and the staggered lattice scale potential generated by the hBN substrate. Numbers in parentheses in sample labels indicate sequential rapid thermal cycling; for example, No 165(2) refers to a second thermal cycle of sample 165.

Received 19 January 2012; accepted 10 April 2012; published online 13 May 2012

References

1. Geim, A. K. & Novoselov, K. S. The rise of graphene. *Nature Mater.* **6,** 183–191 (2007).
2. Ando, T., Fowler, A. B. & Stern, F. Electronic properties of two-dimensional systems. *Rev. Mod. Phys.* **54,** 437–672 (1982).
3. Ezawa, Z. F. *Quantum Hall Effects: Field Theoretical Approach and Related Topics* (World Scientific, 2000).
4. Shayegan, M. *et al.* Two-dimensional electrons occupying multiple valleys in alas. *Phys. Status Solidi.* **243,** 3629–3642 (2006).
5. Goerbig, M. O. Electronic properties of graphene in a strong magnetic field. *Rev. Mod. Phys.* **83,** 1193–1243 (2011).
6. Barlas, Y., Yang, K. & Macdonald, A. Quantum Hall effects in graphene-based two-dimensional electron systems. *Nanotechnology* **12,** 052001 (2012).
7. Nomura, K. & MacDonald, A. H. Quantum Hall ferromagnetism in graphene. *Phys. Rev. Lett.* **96,** 256602 (2006).
8. Zhang, Y. *et al.* Landau-level splitting in graphene in high magnetic fields. *Phys. Rev. Lett.* **96,** 136806 (2006).
9. Jiang, Z., Zhang, Y., Stormer, H. L. & Kim, P. Quantum Hall states near the charge-neutral Dirac point in graphene. *Phys. Rev. Lett.* **99,** 106802 (2007).
10. Checkelsky, J. G., Li, L. & Ong, N. P. Zero-energy state in graphene in a high magnetic field. *Phys. Rev. Lett.* **100,** 206801 (2008).
11. Du, X., Skachko, I., Duerr, F., Luican, A. & Andrei, E. Y. Fractional quantum Hall effect and insulating phase of Dirac electrons in graphene. *Nature* **462,** 192–195 (2009).
12. Dean, C. R. *et al.* Boron nitride substrates for high-quality graphene electronics. *Nature Nanotechnol.* **5,** 722–726 (2010).
13. Dean, C. R. *et al.* Multicomponent fractional quantum Hall effect in graphene. *Nature Phys.* **7,** 693–696 (2011).
14. Yang, K., Das Sarma, S. & MacDonald, A. H. Collective modes and skyrmion excitations in graphene SU(4) quantum Hall ferromagnets. *Phys. Rev. B* **74,** 075423 (2006).
15. Alicea, J. & Fisher, M. P. Interplay between lattice-scale physics and the quantum Hall effect in graphene. *Solid State Commun.* **143,** 504–509 (2007).
16. Goerbig, M. O., Moessner, R. & Douçot, B. Electron interactions in graphene in a strong magnetic field. *Phys. Rev. B* **74,** 161407 (2006).
17. Sheng, L., Sheng, D. N., Haldane, F. D. M. & Balents, L. Odd-integer quantum Hall effect in graphene: Interaction and disorder effects. *Phys. Rev. Lett.* **99,** 196802 (2007).
18. Luk'yanchuk, I. A. & Bratkovsky, A. M. Lattice-induced double-valley degeneracy lifting in graphene by a magnetic field. *Phys. Rev. Lett.* **100,** 176404 (2008).
19. Abanin, D. A., Parameswaran, S. A., Kivelson, S. A. & Sondhi, S. L. Nematic valley ordering in quantum Hall systems. *Phys. Rev. B* **82,** 035428 (2010).
20. Khveshchenko, D. V. Magnetic-field-induced insulating behavior in highly oriented pyrolitic graphite. *Phys. Rev. Lett.* **87,** 206401 (2001).
21. Gorbar, E. V., Gusynin, V. P., Miransky, V. A. & Shovkovy, I. A. Magnetic field driven metal-insulator phase transition in planar systems. *Phys. Rev. B* **66,** 045108 (2002).
22. Abanin, D. A., Lee, P. A. & Levitov, L. S. Spin-filtered edge states and quantum Hall effect in graphene. *Phys. Rev. Lett.* **96,** 176803 (2006).
23. Alicea, J. & Fisher, M. P. A. Graphene integer quantum Hall effect in the ferromagnetic and paramagnetic regimes. *Phys. Rev. B* **74,** 075422 (2006).
24. Gusynin, V. P., Miransky, V. A., Sharapov, S. G. & Shovkovy, I. A. Excitonic gap, phase transition, and quantum Hall effect in graphene. *Phys. Rev. B* **74,** 195429 (2006).
25. Fertig, H. A. & Brey, L. Luttinger liquid at the edge of undoped graphene in a strong magnetic field. *Phys. Rev. Lett.* **97,** 116805 (2006).
26. Fuchs, J-N. & Lederer, P. Spontaneous parity breaking of graphene in the quantum Hall regime. *Phys. Rev. Lett.* **98,** 016803 (2007).
27. Herbut, I. F. Theory of integer quantum Hall effect in graphene. *Phys. Rev. B* **75,** 165411 (2007).
28. Abanin, D. A. *et al.* Dissipative quantum Hall effect in graphene near the Dirac point. *Phys. Rev. Lett.* **98,** 196806 (2007).
29. Jung, J. & MacDonald, A. H. Theory of the magnetic-field-induced insulator in neutral graphene sheets. *Phys. Rev. B* **80,** 235417 (2009).
30. Nomura, K., Ryu, S. & Lee, D-H. Field-induced Kosterlitz–Thouless transition in the $N = 0$ Landau level of graphene. *Phys. Rev. Lett.* **103,** 216801 (2009).
31. Shimshoni, E., Fertig, H. A. & Pai, G. V. Onset of an insulating zero-plateau quantum Hall state in graphene. *Phys. Rev. Lett.* **102,** 206408 (2009).
32. Das Sarma, S. & Yang, K. The enigma of the $\nu = 0$ quantum Hall effect in graphene. *Solid State Commun.* **149,** 1502–1506 (2009).
33. Hou, C-Y., Chamon, C. & Mudry, C. Deconfined fractional electric charges in graphene at high magnetic fields. *Phys. Rev. B* **81,** 075427 (2010).
34. Kharitonov, M. Phase diagram for the $\nu = 0$ quantum Hall state in monolayer graphene. *Phys. Rev. B* **85,** 115439 (2012).
35. Checkelsky, J. G., Li, L. & Ong, N. P. Divergent resistance at the Dirac point in graphene: Evidence for a transition in a high magnetic field. *Phys. Rev. B* **79,** 115434 (2009).
36. Zhang, L. *et al.* Breakdown of the $N = 0$ quantum Hall state in graphene: Two insulating regimes. *Phys. Rev. B* **80,** 241412 (2009).
37. Bolotin, K. I., Ghahari, F., Shulman, M. D., Stormer, H. L. & Kim, P. Observation of the fractional quantum Hall effect in graphene. *Nature* **462,** 196–199 (2009).
38. Zhang, L., Zhang, Y., Khodas, M., Valla, T. & Zaliznyak, I. A. Metal to insulator transition on the $N = 0$ Landau level in graphene. *Phys. Rev. Lett.* **105,** 046804 (2010).
39. Abanin, D. A., Lee, P. A. & Levitov, L. S. Randomness-induced xy ordering in a graphene quantum Hall ferromagnet. *Phys. Rev. Lett.* **98,** 156801 (2007).
40. Aleiner, I. L., Kharzeev, D. E. & Tsvelik, A. M. Spontaneous symmetry breaking in graphene subjected to an in-plane magnetic field. *Phys. Rev. B* **76,** 195415 (2007).
41. König, M. *et al.* Quantum spin Hall insulator state in HgTe quantum wells. *Science* **318,** 766–770 (2007).
42. Nicholas, R. J., Haug, R. J., Klitzing, K. v. & Weimann, G. Exchange enhancement of the spin splitting in a GaAs–$Ga_xAl_{1-x}As$ heterojunction. *Phys. Rev. B* **37,** 1294–1302 (1988).
43. Sondhi, S. L., Karlhede, A., Kivelson, S. A. & Rezayi, E. H. Skyrmions and the crossover from the integer to fractional quantum Hall effect at small Zeeman energies. *Phys. Rev. B* **47,** 16419 (1993).

44. Fertig, H. A., Brey, L., Cote, R. & MacDonald, A. H. Charged spin-texture excitations and the Hartree–Fock approximation in the quantum Hall effect. *Phys. Rev. B* **50,** 11018–11021 (1994).
45. Schmeller, A., Eisenstein, J. P., Pfeiffer, L. N. & West, K. W. Evidence for Skyrmions and single spin flips in the integer quantized Hall effect. *Phys. Rev. Lett.* **75,** 4290–4293 (1995).
46. Nederveen, A. J. & Nazarov, Y. V. Skyrmions in disordered heterostructures. *Phys. Rev. Lett.* **82,** 406–409 (1999).
47. Xue, J. *et al.* Scanning tunnelling microscopy and spectroscopy of ultra-flat graphene on hexagonal boron nitride. *Nature Mater.* **10,** 282–285 (2011).
48. Papic, Z., Goerbig, M. O. & Regnault, N. Atypical fractional quantum Hall effect in graphene at filling factor 1/3. *Phys. Rev. Lett.* **105,** 176802 (2010).
49. Toke, C. & Jain, J. K. Multi-component fractional quantum Hall states in graphene: SU(4) versus SU(2) http://arxiv.org/abs/1105.5270 (2011).
50. Maude, D. K. *et al.* Spin excitations of a two-dimensional electron gas in the limit of vanishing Landé; g factor. *Phys. Rev. Lett.* **77,** 4604 (1996).
51. Shkolnikov, Y. P., Misra, S., Bishop, N. C., De Poortere, E. P. & Shayegan, M. Observation of quantum Hall valley Skyrmions. *Phys. Rev. Lett.* **95,** 066809 (2005).

Acknowledgements

We acknowledge discussions with I. Aleiner, A. Macdonald, Y. Barlas, R. Cote, W. Luo and M. Kharitonov. The measurements were made at NHMFL, which is supported by National Science Foundation Cooperative Agreement DMR-0654118, the State of Florida and the US Department of Energy. We thank S. Hannahs, T. Murphy, J.-H. Park and S. Maier for experimental assistance at NHMFL. This work is supported by the US Defense Advanced Research Projects Agency Carbon Electronics for RF Applications, the Air Force Office of Scientific Research Multidisciplinary University Research Initiative, the Focus Center Research Program through the Center for Circuit and System Solutions and Functional Engineered Nano Architectonics, the Nanoscale Science and Engineering Center (CHE-0117752) and the New York Division of Science, Technology and Innovation. P.K. and A.F.Y. acknowledge support from the US Department of Energy (DE-FG02-05ER46215).

Author contributions

A.F.Y., C.R.D. and P.K. conceived the experiment and analysed the data. A.F.Y., C.R.D., L.W. and H.R. fabricated the samples. A.F.Y., C.R.D., L.W., H.R. and P.C-Z. made the measurements. A.F.Y., C.R.D. and P.K. wrote the paper. T.T. and K.W. synthesized the hBN crystals. J.H., K.L.S. and P.K. advised on experiments.

Additional information

The authors declare no competing financial interests. Supplementary information accompanies this paper on www.nature.com/naturephysics. Reprints and permissions information is available online at www.nature.com/reprints. Correspondence and requests for materials should be addressed to A.F.Y or P.K.